Ocean Modelling 35 (2010) 45–53

Contents lists available at ScienceDirect

Ocean Modelling

journal homepage: www.elsevier.com/locate/ocemod

Background-error correlation model based on the implicit solution of a diffusion equation

Matthew J. Carrier *, Hans Ngodock

Naval Research Laboratory, Stennis Space Center, MS 39529, United States

ARTICLE INFO

Article history:
Received 14 October 2009
Received in revised form 21 May 2010
Accepted 15 June 2010
Available online 3 July 2010

Keywords:
Correlation
Background-error covariance
3D-Var
Data assimilation

ABSTRACT

An efficient implementation of background-error correlation modeling for ocean data assimilation based on the implicit solution of a diffusion equation is presented in this work. This study is an extension of Weaver and Courtier (2001), which sought to model error correlations based on the explicit solution of a generalized diffusion equation. The implicit solution is unconditionally stable, therefore larger time steps can be used in the calculation than in the explicit solution, which needs smaller time steps to maintain stability. This is especially true when modeling anisotropic correlations, or when using a non-uniform model grid (e.g. curvilinear grid spacing). Both implicit and explicit methods are tested in terms of numerical efficiency and practical implementation. To that end, a set of simulated and real data assimilation experiments are carried out using a three-dimensional variational (3D-Var) algorithm that has been developed as a test-bed for these correlation models. The results of both the implicit and explicit method are compared to show that while the implicit method provides the same correlation shape, size, and magnitude as the explicit, it does so at a much lower computational cost. For the experiments shown here the implicit solution can be up to five times as efficient in terms of CPU time than the explicit, while also providing a nearly identical analysis and forecast in terms of deviation from independent observations.

Published by Elsevier Ltd.

1. Introduction

The specification of background error covariances in any assimilation scheme is one of the most important tasks in the field of data assimilation. Until recently, most data assimilation schemes have assumed the structure of the covariances to be isotropic and homogeneous. However, more recent studies suggest that this is a major shortcoming of most data assimilation methods (Kalnay et al., 1997; Houtekamer and Mitchell, 1998; Errico, 1999; Purser et al., 2003b) as this assumption restricts the flow of observational information to circular regions surrounding the measurement location on the analysis grid. Otte et al. (2001) points out that assuming a circular influence region ignores important features such as temperature and wind gradients that may provide valuable information as to the structure of the air mass.

Several studies have been made to investigate the construction of anisotropic and inhomogeneous error correlations on the analysis grid. Purser et al. (2003b) suggest that it is possible to obtain some measure of local anisotropy depending on the geometry of the chosen analysis grid. They point to studies done by Shapiro and Hastings (1973) and Benjamin (1989) who perform an analysis in isentropic coordinates, which provides increased vertical resolution in regions that exhibit high static stability. This approach can be troublesome, however, due to the lack of control on the degree of anisotropy as well as being limited in the variety of shapes one could use. Instead, it has been suggested by numerous studies, most notably by Purser et al. (2003b) and Weaver and Courtier (2001), that to obtain a controllable inhomogeneous and anisotropic structure, one must define an error correlation operator (as a component of the full covariance) with the built-in capability to model these anisotropic features.

Purser et al. (2003a) introduce a method to define a correlation operator based on recursive filters. In this work the filters are purely homogeneous and isotropic. They demonstrate a method to extend the filter algorithm to include anisotropic structures. 3D anisotropic features are captured by utilizing a type of hexad algorithm that applies the filter in the direction of six nonstandard grid lines to achieve some form of "stretching" in the structure functions. This covariance application has been utilized in several studies, most notably in Wu et al. (2002) and Liu et al. (2007) where it was applied in a 3D-Var environment in an effort to assimilate GPS slant-path water vapor observations.

The work in this study is an extension of that done by Weaver and Courtier (2001) who aim to model anisotropic and inhomogeneous correlations for the ocean on a sphere using the diffusion

* Corresponding author. Tel.: +1 228 813 4086.
E-mail address: mcarrier@nrlssc.navy.mil (M.J. Carrier).

1463-5003/$ - see front matter Published by Elsevier Ltd.
doi:10.1016/j.ocemod.2010.06.003

equation. Weaver and Courtier (2001) build on previous studies done by Egbert et al. (1994) and Derber and Rosati (1989) who proposed the use of an iterative Laplacian grid-point filter to build error correlations. In the case of Weaver and Courtier (2001) the Laplacian operator is interpreted to be a time-step integration of a diffusion equation, where the integral kernel of the equation is the representation of a covariance function. Their work demonstrates the ability to model anisotropic correlations by defining the diffusion coefficient as a function of the analysis grid. This method has been employed successfully in numerous studies, including Weaver et al. (2003), Ngodock (2005), Weaver et al. (2005), and Pannekoucke and Massart (2008).

Weaver and Courtier (2001) base their method on the explicit solution to a generalized diffusion equation. A consequence of this is that the correlation operator is only conditionally stable. Depending on the degree of anisotropy in the correlation structures, this method could require several hundred or even thousands of time stepping iterations to produce a correlation field due to the CFL stability criterion. Purser et al. (2003b) point out that one of the main advantages of their filter approach is the relative speed in comparison to the diffusion method.

The work presented in here illustrates the use of the implicit solution to a diffusion equation to increase the computational efficiency of the Weaver and Courtier (2001) algorithm. In the next section a detailed examination of the implicit-solution scheme is presented as well as a general comparison between the correlation shapes produced from the implicit and explicit solutions of the diffusion equation. Section three then outlines the set-up and results for both the simulated and the real data assimilation experiments in the Monterey Bay and Hawaiian regions, respectively. These experiments demonstrate the usefulness of the error correlation operator in a three-dimensional variational (3D-Var) assimilation algorithm and illustrate the advantage of using the implicit solution to the diffusion equation rather than the explicit. Section four summarizes the presented work and provides a brief discussion of the intended future work.

2. The background-error correlation operator

Weaver and Courtier (2001; hereto WC2001) based their work on that done by Derber and Rosati (1989) who demonstrate that an iterative Laplacian grid-point filter can be used to model correlations. One application of this approach assumes that the Laplacian filter be viewed as a time-step integration of a diffusion equation (Egbert et al., 1994; Bennett et al., 1997). WC2001 build on this approach to define 2D and 3D univariate correlation models that are not only efficient in terms of computational speed, but also provide a method for constructing anisotropic and inhomogeneous correlations. For a more complete description of this error correlation operator, the authors refer the reader to WC2001.

2.1. Correlation operator using the implicit solution of a diffusion equation

As noted, the correlation operator is built upon the solution to the standard diffusion equation:

$$\frac{\partial \eta}{\partial t} = \nabla \cdot (\kappa \nabla \eta), \tag{1}$$

where the diffusion coefficient is a spatially varying quantity and therefore can be used to modify the length scale and shape of the correlation based on any predetermined field; it should be noted that the Laplacian operator is three-dimensional. The explicit solution of (1) is of the form:

$$\eta^{n+1} = \eta^n + \Delta t \nabla \cdot (\kappa \nabla \eta^n). \tag{2}$$

It can be proved that in order to maintain stability the time step (M) should be set as $M \geqslant 2(L/e)^2$, where L is the correlation length scale and e the horizontal grid resolution. This requirement in the explicit solution affects the computational cost of modeling anisotropic and inhomogeneous correlations. The result is a dramatic increase in computational time for the explicit solution since M would need to be computed using the ratio of the largest correlation length scale value to the horizontal grid step ($L_{\max}/e$). Due to this, we introduce another approach to solve for (1) using an implicit scheme. Here, the solution to (1) can be written as

$$\eta^{n+1} = \eta^n + \Delta t \nabla \cdot (\kappa \nabla \eta^{n+1}). \tag{3}$$

The solution (3) is unconditionally stable and does not require prohibitively small time steps for integration (Weaver and Ricci, 2004). From (3) if $A = \Delta t \nabla \cdot (\kappa \nabla)$, then Eq. (3) can be re-arranged to the form,

$$(I - A)\eta^{n+1} = \eta^n, \tag{4}$$

which can be solved using a conjugate gradient algorithm. Using (4) for the filter design reduces the computational time required over the explicit solution. Using the conjugate gradient for solving (4) requires a stopping criterion for convergence. A series of experiments have been done to investigate the impact of the convergence criterion on the solution. Experiments with stringent convergence criterion (residual less than 1.0×10^{-5}) have displayed no substantial gain when compared to looser criterion. It can be shown that any value of the residual between 1.0×10^{-2} and 1.0×10^{-5} can provide adequately accurate results (as defined by a comparison to the explicit-solution operator), however, it should be noted that a residual value of 1.0×10^{-1} has been found to be inadequate for the purposes of this correlation operator. For the work shown here, a residual criterion of 1.0×10^{-5} has been selected as a balance between accuracy and efficiency; however a looser criterion could have also been used and would have afforded an even greater cost savings over the explicit-solution operator than is shown here.

The explicit and implicit solutions are approximations of the true solution to the diffusion equation. The difference between the approximation and the true solution is related to the size of the time step used to solve the equation either implicitly or explicitly; this difference is known as truncation error. Since the implicit solution normally uses a larger time step than the explicit solution, these two operators will provide slightly different results. This can be mitigated by applying the implicit-solution correlation operator numerous times, thereby shortening the time step used. This does result in an increase in the computational cost of the operator, however not so much as to eliminate the cost savings over the explicit-solution operator. For the results shown in this work, the implicit-solution operator has been applied ten times in order to closely approximate the results of the explicit-solution operator. Fig. 1 compares the CPU time used to run the explicit solution (red) and implicit solution (dashed blue) for a selected test case. This experiment involves an arbitrary 3D grid of $157 \times 130 \times 46$ with a resolution of 1 km. A total of 4250 Dirac impulses, at various horizontal and vertical positions, are passed through both filters. The computer codes for these operators are both currently serial versions and are run on one Opteron 2200 2.8 GHz processor. The grid resolution is fixed at 1 km, however six different horizontal length scale values are used: 5 km, 10 km, 20 km, 30 km, 40 km, and 50 km. Fig. 1 shows that the CPU time for the explicit solution rises rapidly, whereas the CPU time for the implicit solution increases at a much lower, nearly linear rate.

It should be noted that the algorithm also employs a set of normalization factors to ensure that the solution of the algorithm is, in fact, a correlation field. Any number of methods can be employed to calculate the normalization factors such as an explicit

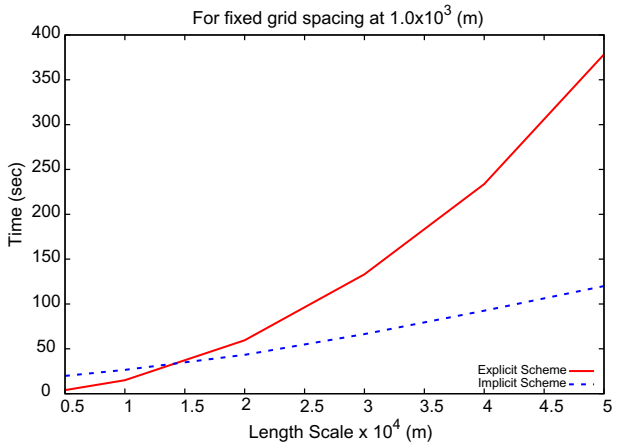

Fig. 1. CPU time to run diffusion-based correlation operator for a fixed grid resolution and varying correlation length scales. Implicit solver in dashed blue, explicit in solid red; *y*-axis is CPU time (in seconds) and *x*-axis is correlation length scale (in 10^4 m). (For interpretation of the references to colour in this figure legend, the reader is referred to the web version of this article.)

calculation or Monte Carlo techniques. The normalization factors would then be applied to the algorithm as in Weaver and Ricci (2004). Fig. 2 shows a side-by-side comparison of an error correlation in an arbitrary grid where a set of normalization factors have been used. Fig. 2a (Fig. 2b) shows the correlation constructed using the explicit (implicit) solution. In both figures the horizontal grid is 157×130 with a length scale of 60 km and a resolution of 6 km; no length scale modification is used. The implicit solution produces a correlation with nearly identical shape, size, and magnitude as the explicit solution. The difference field is shown in Fig. 2c.

To demonstrate that these two methods produce similar results when simulating anisotropic correlations, an empirical length scale modification is employed that accounts for the changes in bathymetry. It has been suggested that correlations become horizontally stretched in the along shore direction when near a coastline boundary (Li et al., 2008; Weaver and Ricci, 2004) in shallow water. This anisotropic feature can be approximated using a quadratic function of bathymetry,

$$\kappa_{i,j,k} = c(D - d_{i,j,k})^2 + 1, \tag{5}$$

where $\kappa_{i,j,k}$ is the set of spatially varying diffusion coefficients, D defines the maximum depth of the water column where correlation stretching will occur (model grid points with depths greater than D will be isotropic), and $d_{i,j,k}$ is the depth at model grid point (i, j, k). It should be noted that the minimum value of κ is never allowed

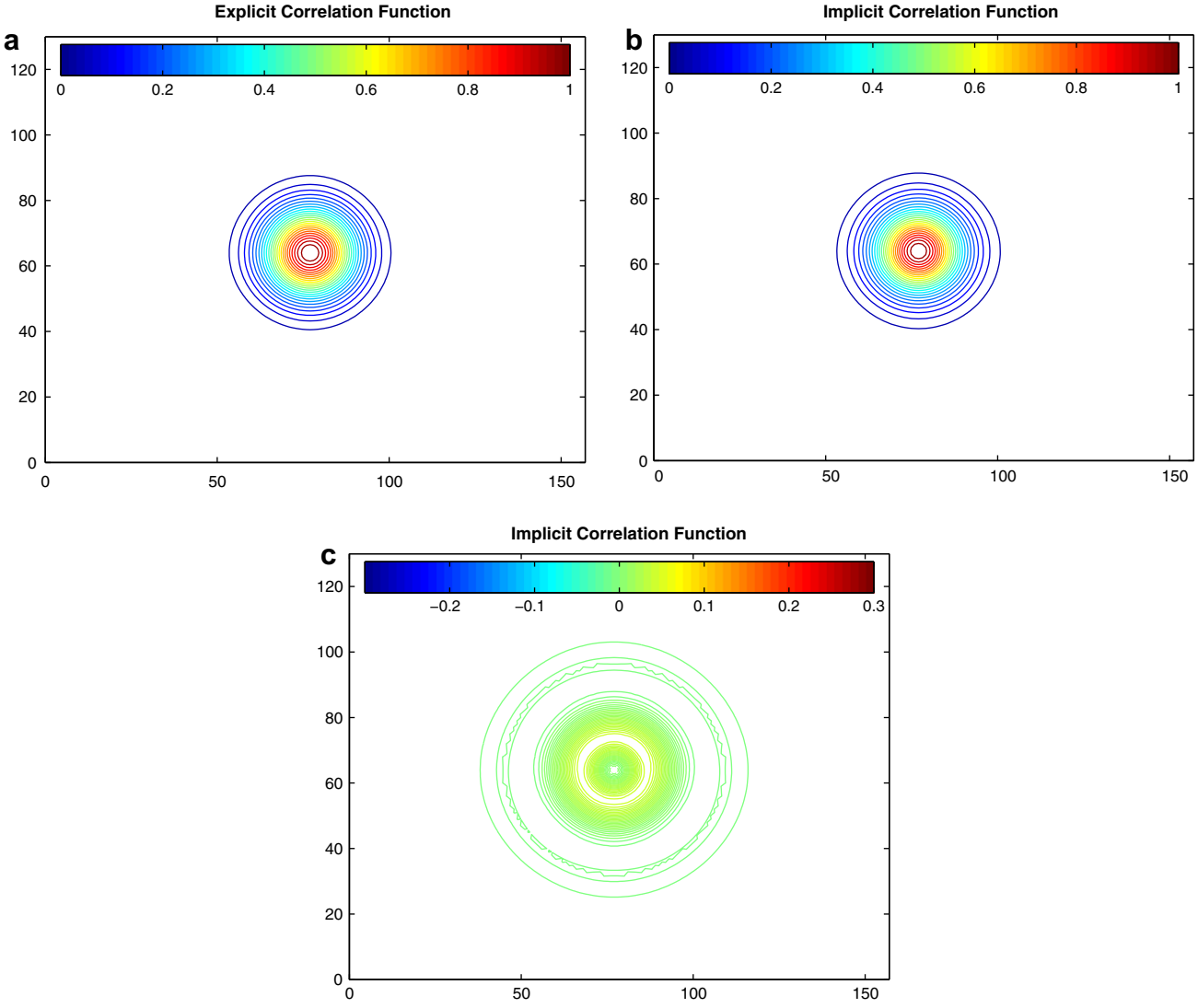

Fig. 2. Example correlation function centered at 78×65 on arbitrary grid; center value is 1.0 for (a) the explicit solver, (b) the implicit solver and (c) displays the difference field explicit minus implicit. Grid resolution and correlation length scale are fixed at 6.0×10^3 m and 6.0×10^4 m, respectively.

to go below 1.0 and its maximum value is capped at 5.0 by the constant c. This constant is calculated as the maximum diffusion coefficient value (κ^{max}) minus the minimum value (κ^{min}) normalized by the square of D. Fig. 3 shows the side-by-side comparison of an error correlation using this length scale modification feature with Fig. 3a (Fig. 3b) using the explicit (implicit) solution. The difference field is shown in Fig. 3c. In this case, an actual geographical region is needed with a land mass within the model domain. Here, a near-shore example around Monterey Bay, California is used with a $81 \times 58 \times 41$ grid and 1 km horizontal grid resolution. Both correlations exhibit obvious along-shore stretching in relation to the relatively shallow coastal bathymetry, shown in Fig. 3d.

3. Assimilation scheme and experiments

Testing a new error covariance scheme is an intensive and time consuming project. Such validation normally requires many months of trials involving numerous real-data experiments from a variety of oceanic conditions and regimes. Conducting this sort of validation is beyond the scope of this study. However, two experiments are presented here: (1) a simulated and (2) real-data experiment to demonstrate the capabilities of this implicit solution background-error correlation operator in a data assimilation environment.

3.1. Assimilation scheme and forecast model

For these experiments the three-dimensional variational (3D-Var) analysis scheme is utilized. The analysis equation employed is the following

$$\mathbf{x}_a = \mathbf{x}_b + \mathbf{B}\mathbf{H}^{\mathbf{T}}(\mathbf{H}\mathbf{B}\mathbf{H}^{\mathbf{T}} + \mathbf{R})^{-1}(\mathbf{y} - \mathbf{H}\mathbf{x}_b), \tag{6}$$

where each variable follows the conventional definition. For simplicity $\mathbf{R}$ is taken as the diagonal matrix containing only the observation variances.

The oceanic forecast model is the Navy Coastal Ocean Model (NCOM) and is capable of producing ocean forecasts of temperature, salinity, sea surface height, and velocity for regional near-shore environments or for the global oceans (Martin, 2000). The model has a free surface and is based on the primitive equations. Surface forcing conditions (e.g. wind stress, infrared radiation flux,

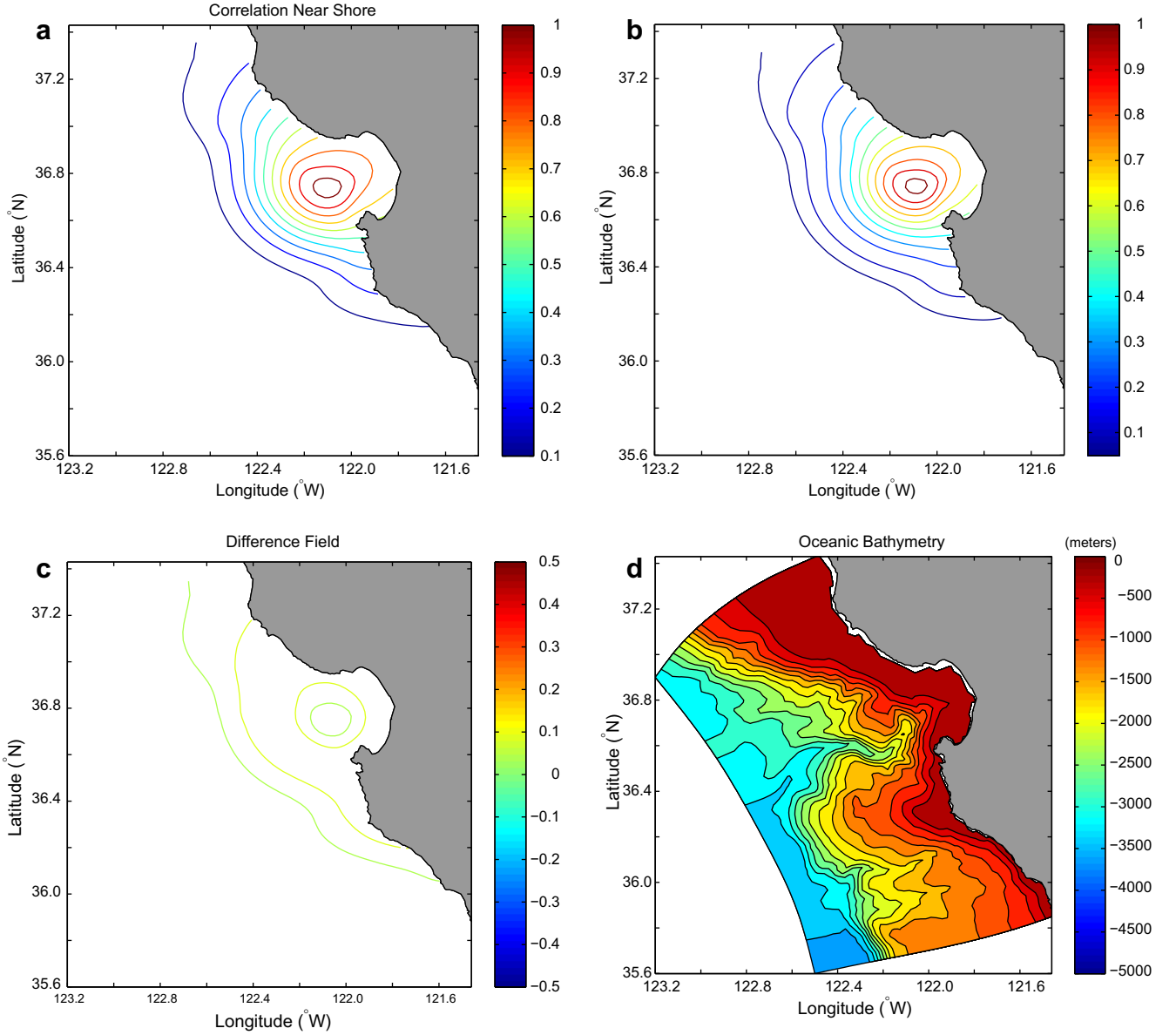

Fig. 3. Anisotropic correlation function (with length scale modification) near the coast of Monterey Bay, California, USA using the (a) explicit, (b) implicit solver, (c) shows the difference field explicit minus implicit, and (d) shows the bathymetry.

etc.) are provided by the global Navy Operational Global Atmospheric Prediction System (NOGAPS, Rosmond et al., 2002) with 0.5° horizontal grid resolution. The NOGAPS forcings are archived every 12 h at the synoptic times of 0000 and 1200 UTC.

3.2. Monterey Bay simulated data assimilation

3.2.1. Experiment design

This experiment involves simulated data for a Monterey Bay simulation. Here the NCOM model has an $81 \times 57 \times 41$ grid with a variable horizontal grid resolution between 1 km and 4 km. For this experiment two NCOM forecasts are run, one during the time frame of January, 2007 and the second for the following month of February, 2007. For the sake of this discussion, the January forecast will be referred to as the control (CTRL) and the February forecast as the observations (OBS). Model profile data of temperature and salinity are selected at 24-h intervals from the OBS model run at 13 locations (Fig. 4) throughout the grid. A low number of profile data locations is selected to mimic the sparse distribution of real-world profile observations. Data from OBS are assimilated in a 24-h update cycle and the resulting analysis is used to run another NCOM forecast for January, 2007; OBS data from February 1st is assimilated into the analysis for January 1st; OBS data from February 2nd is assimilated into the analysis for January 2nd, and so on. This forecast will be referred to as the optimal forecast (3DV). Here, there are two optimal forecasts performed, one using an analysis created with the explicit-solution correlation operator (3DV-EXP) and one with the implicit-solution correlation operator (3DV-IMP). Both analyses are evaluated by examining the difference fields between the 3DV forecasts and the OBS forecast at non-assimilated locations. And the overall forecast is evaluated using a normalized error metric, which is developed to evaluate many aspects of these experiments, and is a relative measurement of either the analysis or forecast error through time. The metric e_b is defined as

$$e_b = \left(\frac{\sum_{k=1}^{K} \frac{\left(\mathbf{H}\mathbf{x}_b^k - \mathbf{y}^k\right)^2}{\sigma_{\text{obs}}^2}}{K} \right), \tag{7}$$

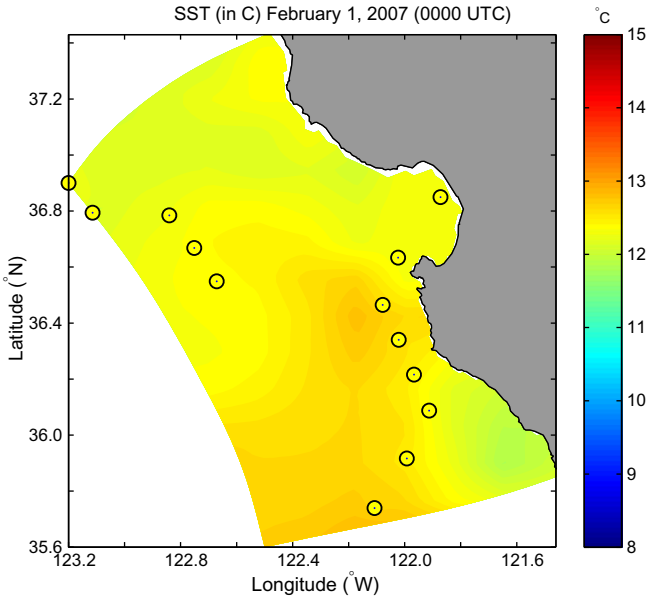

Fig. 4. 13 T/S profile locations selected in NCOM domain for simulated ocean data assimilation experiment. Field shown is SST (in °C) for 1 February, 2007 at 0000 UTC.

where k is the observation index, $\mathbf{x}_b^k$ is the model state (mapped to the observation space by $\mathbf{H}$), $\mathbf{y}^k$ is the observation, σ_{obs}^2 is the observation variance. The metric is computed as a time series at each 24-h time level and each 24-h value is normalized by the initial value at $t = 0$. In order to compare results, both the 3DV-IMP and the 3DV-EXP results have been normalized by the $t = 0$ values from the 3DV-IMP experiment. It should be noted that the correlation length scale is based on the Rossby radius of deformation and is variable between 20 and 30 km.

3.2.2. Experiment results

Fig. 5 shows a time evolution (six-panel plot) of the 3DV minus OBS (analysis minus observation) profile difference for temperature (T) at a non-assimilated model grid point. The closest selected assimilated OBS point to this profile location is 12 km. The CTRL profile is shown in red, the 3DV-IMP in green, and the 3DV-EXP in blue. The six panels show the profile for the initial time (day 1) then days 5, 10, 15, 20, and 25. The 3DV-EXP and 3DV-IMP profiles are remarkably similar, as the difference in correlation operator does not produce diverging results. Also, the T difference is reduced significantly in the 3DV results when compared to the CTRL. The analysis seems to be better at depth than near the surface, but this is likely due to the fact that the ocean is more variable near the surface (due to prevailing surface forcing conditions). Nevertheless, the 3DV results (both implicit and explicit) show improvement in the near surface T difference when compared to the CTRL results. Fig. 6 shows this same profile time evolution for salinity (S). The results shown for this profile are representative of the entire model solution (all profiles).

Fig. 7 shows the normalized error metric for the full 28-day 3DV forecast. The T error is shown in red, S in blue, and total velocity (V) in green. The 3DV-IMP (3DV-EXP) results are shown as the solid lines (dashed lines). It is clear that as the 24-h update assimilation cycle continues through the 28-day forecast, the errors for all fields decrease dramatically. The largest decrease occurs in the first ten days as the errors in most fields drop from 1.0 to 0.3–0.4. Also, it is worth noting that the 3DV-IMP and 3DV-EXP results are nearly identical.

The timing results for this experiment indicate the improved computational efficiency of the implicit-solution correlation operator over the explicit version. For the experiment utilizing the explicit-solution correlation operator, the full 28-day analysis-forecast cycle ran in 128 min using a single-processor Opteron 2200 2.8 GHz computer, whereas the version using the implicit-solution correlation operator took just under an hour at 42 min, a savings ratio of roughly 3:1.

3.3. RIMPAC real data assimilation

3.3.1. Experiment design

The real data assimilation experiment concerns a geographical region surrounding the Hawaiian island chain during a 15-day period from 16 June to 30 June, 2008. The NCOM grid used for this experiment is $157 \times 130 \times 46$ with a 6 km grid resolution with boundary conditions supplied from the operational global NCOM run. Observations are selected from a portion of the Navy's RIMPAC (Rim of the Pacific) exercise with a 24-h update cycle used to assimilate the observations at 0000 UTC each day; assimilated data are collected from a +/− 12-h window around the analysis time. This 3D-Var routine is linked directly to the observation preparatory and quality control program suite from the Navy Coupled Ocean Data Assimilation (NCODA) system, known as NCODA-prep (Cummings, 2005). This was done to ensure that the included observations were of operational quality and to take advantage of the well-established data selection and quality control routines already included in the NCODA system.

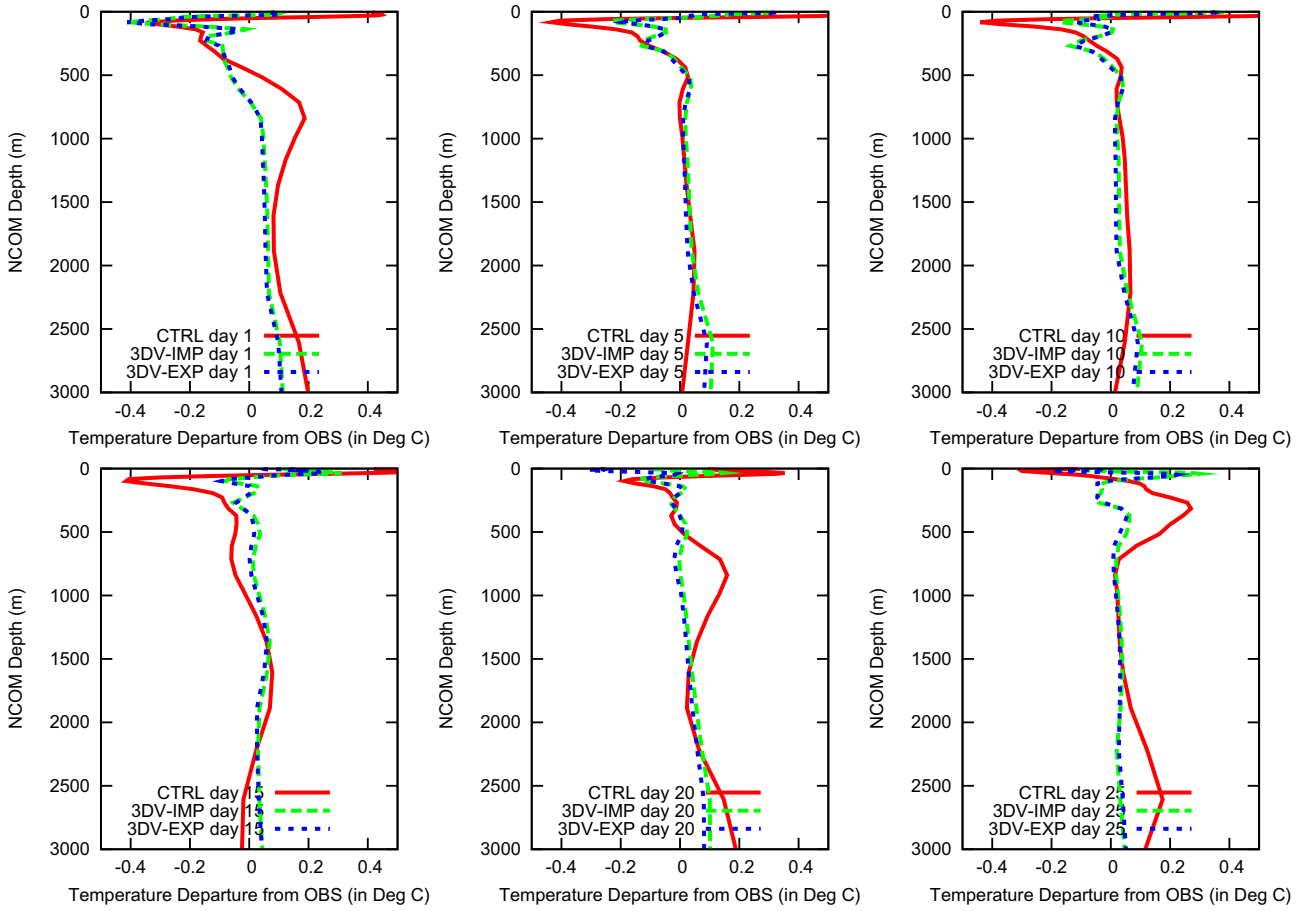

Fig. 5. CTRL minus OBS (solid red), 3DV-IMP minus OBS (dash green), and 3DV-EXP minus OBS (dash blue) temperature difference at the initial time and at days 5, 10, 15, and 25 for an NCOM grid point within 12 km of a nearby observation location. (For interpretation of the references to colour in this figure legend, the reader is referred to the web version of this article.)

The observational data used for this experiment include many sources such as oceanic gliders (Rudnick et al., 2004), ARGO float profiles (Roemmich et al., 2001), and Modular Ocean Data Assimilation System synthetics profiles (MODAS, Fox et al., 2002), however only three variables are considered in the analysis: *T*, *S* (surface and sub-surface), and *SSH*. The background error variances are calculated as in Cummings (2005). As in the simulated data experiment, two assimilation model runs are conducted here. One uses a 3D-Var with the implicit correlation operator (IMPL) and the other with the explicit operator (EXPL).

3.3.2. Experiment results

To investigate the analysis, four observational profiles of *T* and *S* have been excluded from each of the assimilation cycles to be used as independent observations for validation purposes; results from one profile location are shown here. The location of this profile is shown relative to other observation data in Fig. 8 (red cross) for 16 June, 2008. It should be noted that this figure includes the location of surface-only (black dots) and profile observation locations (red dots). The observation profiles are compared to profiles from three model runs: (1) the first guess (FG) field, (2) a 3D-Var analysis using the implicit-solution correlation operator (IMPL), and (3) a 3D-Var analysis using the explicit-solution correlation operator (EXPL). As in the simulated data experiment, the Rossby radius of deformation is used here to define the correlation length scale, resulting in correlation length scales ranging from 55 to 70 km.

Fig. 9 shows a comparison between three model profiles (from FG, IMPL, and EXPL) and one non-assimilated observation profile at 0000 UTC 16 June, 2008. Absolute differences are calculated between the observation value and FG (red), IMPL (green), and EXPL (blue) for *T* (Fig. 9a) and *S* (Fig. 9b). The FG field features a large discrepancy with the observation value for both *T* and *S* for just below the surface to around 500 m. This region has been identified as the mixed layer (figure omitted), and suggests that NCOM is having some difficulty correctly simulating the thermodynamic properties of this layer. This discrepancy is reduced significantly in the IMPL and EXPL results, even though the nearest assimilated profile observation in this analysis is at 42 km distance.

The IMPL and EXPL difference profiles are very similar, especially in the *S* values. The *T* difference profiles show some dissimilarities, however these are small, on order of about 0.05 °C. These differences, however, have little impact on the overall structure of the analysis and on the performance of the resulting forecast (to be shown later). It is important to note that the results from the other withheld profiles, for all time levels, are similar to the example shown here.

A brief assessment of the real data forecast, using the 3D-Var analysis, is shown in Fig. 10 using error metric (7). The *T* error is in red, *S* error in blue, *SSH* error in green, and the IMPL (EXPL) results are shown as solid (dashed) lines. Clearly the errors in all fields are nearly identical between the IMPL and EXPL model runs. The error generally decreases as the forecast progresses, indicating that the assimilation of observations is having a positive impact on

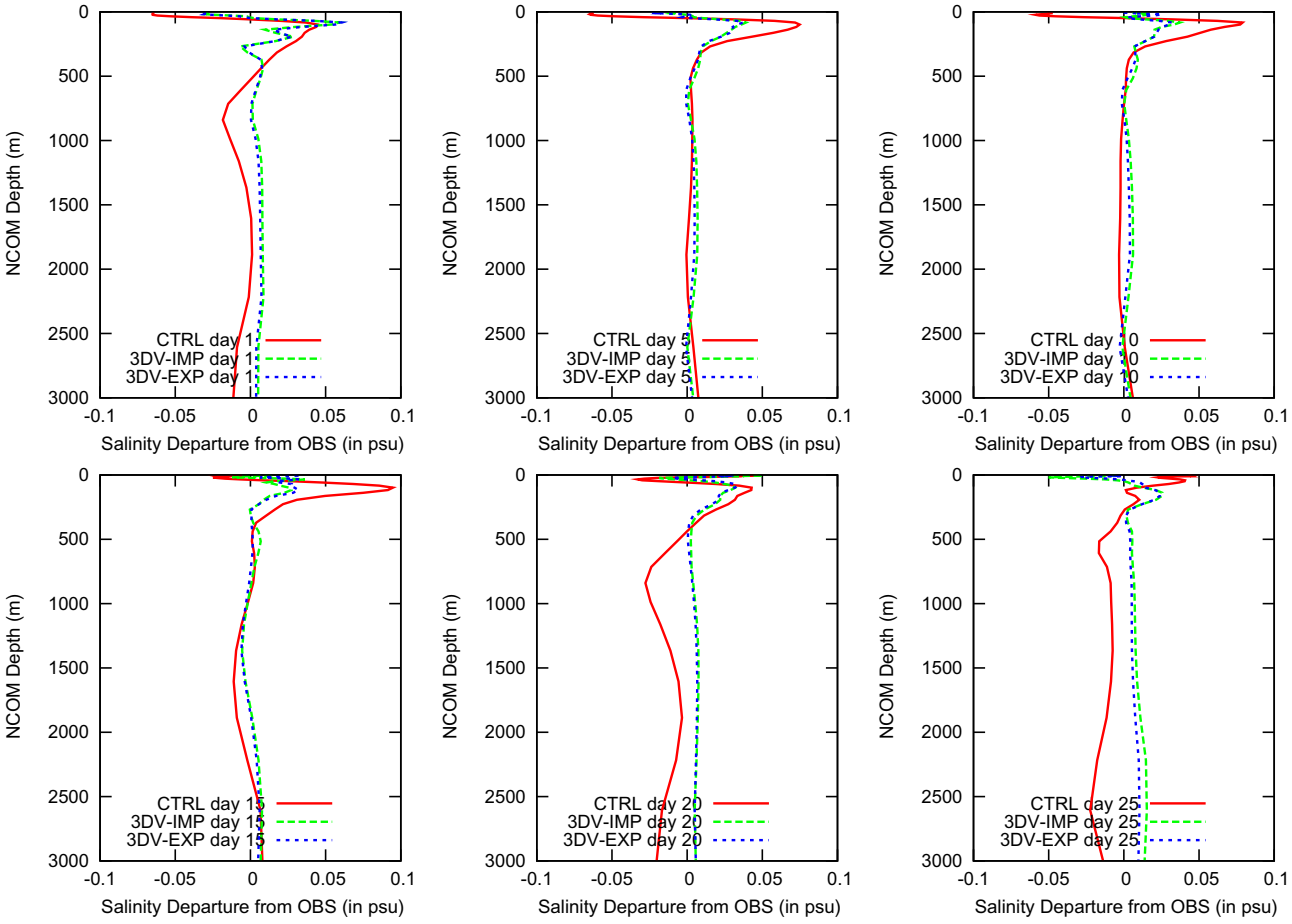

Fig. 6. Same as in Fig. 5, but for salinity.

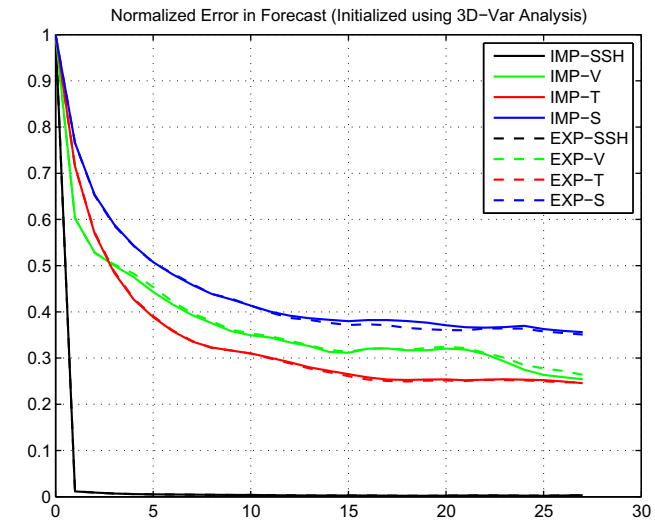

Fig. 7. Relative forecast error in T (red), S (blue), and total v (green) for 3DV-IMP (solid) and 3DV-EXP (dashed). Relative error is normalized by error in each field at day 1. Error is calculated as in (8). (For interpretation of the references to colour in this figure legend, the reader is referred to the web version of this article.)

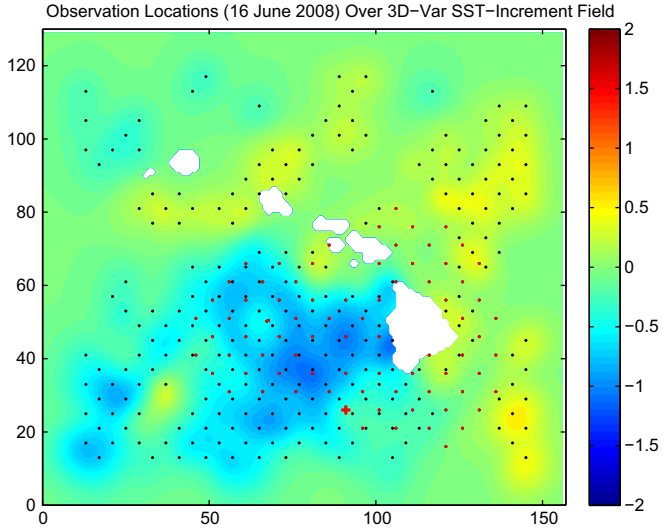

Fig. 8. All temperature observation locations for 16 June, 2008 including surface observations (black dots) and profile observations (red dots) overlaid on 3D-Var surface temperature increments. Location of excluded profile used as independent observation indicated by red cross. (For interpretation of the references to colour in this figure legend, the reader is referred to the web version of this article.)

the analysis and the resulting forecast. There appears to be little statistical difference between the two forecasts, save for the amount of CPU time required to run the two systems. For this real-data experiment in the RIMPAC region the 3D-Var using the IMPL out-performs the EXPL nearly 5:1, at 4 h to the EXPL's 18 h (using a single-processor Opteron 2200 2.8 GHz computer).

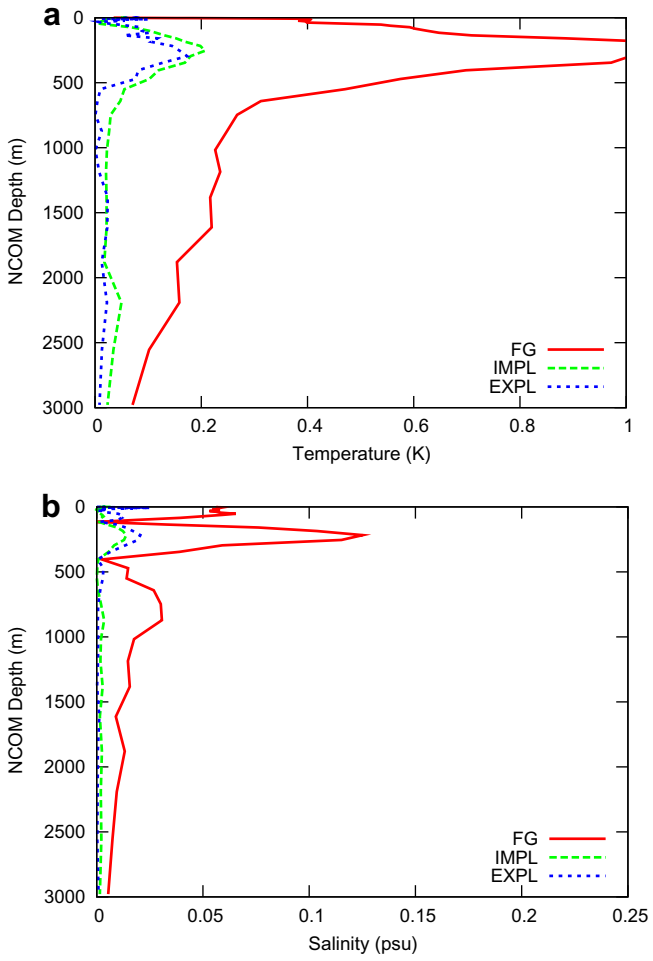

Fig. 9. Absolute difference between observation profile and first guess (FG) profile (red), analysis that used the implicit-solution correlation operator (green), and analysis that used the explicit operator (blue). Left (a) is for temperature, panel (b) is for salinity. Comparison is valid at 0000 UTC 16 June, 2008. (For interpretation of the references to colour in this figure legend, the reader is referred to the web version of this article.)

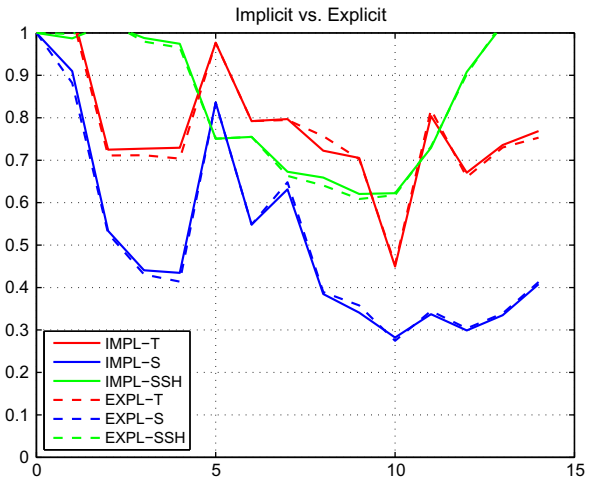

Fig. 10. Relative forecast error in *T* (red), *S* (blue) and *SSH* (green) for IMPL model run (solid) and EXPL model run (dashed). Relative error is normalized by error in each field at day 1. Error is calculated as in (8). (For interpretation of the references to colour in this figure legend, the reader is referred to the web version of this article.)

Clearly, this represents a significant savings in terms of computational time and resources.

4. Summary and future work

An alternative method of error correlation modeling based on a diffusion equation has been presented. It is known that a correlation operator relying on the explicit solution to a diffusion equation is conditionally stable, thereby limiting the size of the time step in order to maintain stability. This is especially true of modeling anisotropic correlations where the correlation length scale changes spatially over a model grid with fixed resolution. In this case, the explicit-solution correlation operator requires a large number of small time steps in order to maintain stability. On the other hand, the implicit-solution correlation operator is unconditionally stable and does not require a drastic increase in computational time to handle any correlation shape that may be desired.

Comparisons between the explicit and implicit-solution correlation operators demonstrate that the implicit solution produces correlations very similar to the explicit solution in terms of magnitude, shape, and spatial size. The performance of the operators is shown in terms of both simulated and real data assimilation experiments. In the real-data experiment, observations collected by the NCODA preparation subroutines are used in a 15 day forecast, in which a 24-h forecast cycle assimilates data daily at 0000 UTC. Here observational profiles of temperature and salinity are withheld at four locations in each assimilation cycle; these profiles are then used to evaluate the performance of the assimilation scheme and the correlation operators. The results suggest that the correlation operators perform well in spreading information from the observations throughout the model grid, and to locations where no data are assimilated. Also, the results from the RIMPAC real-data experiment show that the implicit and explicit-solution operators provide nearly identical results in the 3D-Var system; however, the 3D-Var using the implicit-solution correlation operator ran in approximately 1/5 the time of the system employing the explicit operator.

The next step in this research is to perform a more robust validation of this implicit covariance operator. This would involve testing the performance of the operator in real data assimilation experiments involving numerous environmental regimes (i.e. deep water, near shore, strong upwelling/downwelling, presence of fronts, etc.) to assess how well the system adapts to changing conditions.

Acknowledgements

This work was sponsored by the Office of Naval Research Program Element No. 0601153N as part of the Projects "Exploring Covariances for Ocean Variational Data Assimilation" and "Variational Data Assimilation for Ocean Prediction." This paper is the Naval Research Laboratory paper contribution number JA/7320-08-9061.

References

Benjamin, S.G., 1989. An isentropic meso-α-scale analysis system and its sensitivity to aircraft and surface observations. Mon. Weather. Rev. 117, 1586–1603.

Bennett, A.F., Chua, B.S., Leslie, L.M., 1997. Generalized inversion of a global numerical weather prediction model, II: Analysis and implementation. Meteorol. Atmos. Phys. 62, 129–140.

Cummings, J.A., 2005. Operational multivariate ocean data assimilation. Quart. J. Roy. Meteorol. Soc. 131, 3583–3604.

Derber, J., Rosati, A., 1989. A global oceanic data assimilation system. J. Phys. Oceanogr. 19, 1333–1347.

Egbert, G.D., Bennett, A.F., Foreman, M.G.G., 1994. Topex/Poseidon tides estimated using a global inverse model. J. Geophys. Res. 99, 24821–24852.

Errico, R.M., 1999. Meeting summary: workshop on assimilation of satellite data. Bull. Am. Meteorol. Soc. 80, 463–471.
Fox, D.N., Teague, W.J., Barron, C.N., 2002. The modular ocean data assimilation system (MODAS). J. Atmos. Ocean. Technol. 19, 240–252.
Houtekamer, P.L., Mitchell, H.L., 1998. Data assimilation using an ensemble Kalman filter technique. Mon. Weather Rev. 126, 796–811.
Kalnay, E. et al., 1997. Data assimilation in the ocean and atmosphere: what should be next? J. Meteorol. Soc. Jpn. 75, 489–496.
Li, Z., Chao, Y., McWilliams, J.C., Ide, K., 2008. A three-dimensional variational data assimilation scheme for the Regional Ocean Modeling System. J. Atmos. Ocean. Technol. Early Online Release. doi:10.1175/2008JAS2647.1.
Liu, H., Xue, M., Purser, R.J., Parrish, D.F., 2007. Retrieval of moisture from simulated GPS slant-path water vapor observations using 3DVAR with anisotropic recursive filters. Mon. Weather Rev. 135, 1506–1521.
Martin, P.J., 2000. Description of the Navy Coastal Ocean Model Version 1.0. NRL Rep. NRL/FR/7322/00/9962, 45 pp. [Available from NRL, Code 7322, Bldg. 1009, Stennis Space Center, MS 39529-5004].
Ngodock, H.E., 2005. Efficient implementation of covariance multiplication for data assimilation with the representer method. Ocean Mod. 8, 237–251.
Otte, T.L., Seaman, N.L., Stauffer, D.R., 2001. A heuristic study on the importance of anisotropic error distributions in data assimilation. Mon. Weather Rev. 129, 766–783.
Pannekoucke, O., Massart, S., 2008. Estimation of the local diffusion tensor and normalization for heterogeneous correlation modelling using a diffusion equation. Quart. J. Roy. Meteorol. Soc. 134, 1425–1438.
Purser, R.J., Wu, W.S., Parrish, D.F., Roberts, N.M., 2003a. Numerical aspects of the application of recursive filters to variational statistical analysis. Part I: Spatially homogeneous and isotropic Gaussian covariances. Mon. Weather Rev. 131, 1524–1535.
Purser, R.J., Wu, W.S., Parrish, D.F., Roberts, N.M., 2003b. Numerical aspects of the application of recursive filters to variational statistical analysis. Part II. Spatially inhomogeneous and anisotropic general covariances. Mon. Weather Rev. 131, 1536–1548.
Roemmich, D. et al., 2001. Argo: The global array of profiling floats. In: Koblinsky, C.J., Smith, N.R. (Eds.), Observing the Oceans in the 21st Century. Melbourne Bureau of Meteorology, 604 pp.
Rosmond, T.E., Teixeira, J., Peng, M., Hogan, T.F., Pauley, R., 2002. Navy operational global prediction system (NOGAPS): forcing for ocean models. Oceanography 15, 99–106.
Rudnick, D.L. et al., 2004. Underwater gliders for ocean research. Marine Technology Society Journal 38, 48–59.
Shapiro, M.A., Hastings, J.T., 1973. Objective cross section analysis by Hermite polynomial interpolation on isentropic surfaces. J. Appl. Meteorol. 12, 753–762.
Weaver, A., Courtier, P., 2001. Correlation modeling on the sphere using a generalized diffusion equation. Quart. J. Roy. Meteorol. Soc. 127, 1815–1846.
Weaver, A.T., Vialard, J., Anderson, D.L.T., 2003. Three- and four-dimensional variational assimilation with a general circulation model of the tropical Pacific ocean. Part I: Formulation, internal diagnostics, and consistency checks. Mon. Weather Rev. 131, 1360–1378.
Weaver, A., Ricci, S., 2004. Constructing a background-error correlation model using generalized diffusion operators. In: ECMWF Seminar on Recent Developments in Data Assimilation for Atmosphere and Ocean, Reading, UK, 8–12 September, European Centre for Medium-Range Weather Forecasts.
Weaver, A.T., Deltel, C., Machu, E., Ricci, S., Daget, N., 2005. A multivariate balance operator for variational ocean data assimilation. Quart. J. Roy. Meteorol. Soc. 131, 3605–3625.
Wu, W.S., Purser, R.J., Parrish, D.F., 2002. Three-dimensional variational analysis with spatially inhomogeneous covariances. Mon. Weather Rev. 130, 2905–2916.